Fabrication of three-dimensional sin-shaped ripples using a multi-tip diamond tool based on the force modulation approach

Yuzhang Wang[1,2], Pengfei Fan[3], Xichun Luo[3], Yanquan Geng[1,2], Saurav Goel[4,5,6,7], Wei Wu[8], Guo Li[9] and Yongda Yan[1,2*]

[1] *Key Laboratory of Micro-systems and Micro-structures Manufacturing of Ministry of Education, Harbin Institute of Technology, Harbin, Heilongjiang 150001, P.R. China*

[2] *Center for Precision Engineering, Harbin Institute of Technology, Harbin, Heilongjiang 150001, P.R. China*

[3] *Centre for Precision Manufacturing, DMEM, University of Strathclyde, Glasgow, G1 1XQ, UK*

[4] *London South Bank University, 103 Borough Road, London, SE1 0AA, UK*

[5] *Shiv Nadar University, Gautam Budh Nagar, 201314, India*

[6] *Indian Institute of Technology Guwahati, Guwahati, 781039, India*

[7] *University of Petroleum and Energy Studies, Dehradun, 248007, India*

[8] *Key Laboratory of Weak-Light Nonlinear Photonics of Ministry of Education, TEDA Institute of Applied Physics and School of Physics, Nankai University,Tianjin 300457, P.R. China*

[9] *Research Center of Laser Fusion, China Academy of Engineering Physics, Mianyang, Sichuan 621900, P.R. China*

** Corresponding author. Tel.: +86-451-86412924. Fax: +86-451-86415244*

E-mail address: yanyongda@hit.edu.cn (Y. D. Yan)

Abstract

A novel cutting strategy of machining microstructure surface with the multi-tip diamond tool based on the force modulation approach is proposed in this paper. The multi-tip diamond tool with periodic sinusoidal microstructures was prepared by focused ion beam technique. The influence of applied cutting forces on the depths of cut and material removal states was investigated experimentally. MD simulations

revealed a significant phenomenon of no material side flow when using the multi-tip diamond tool cutting on single crystal copper substrate. The movement of stacking faults, Lomer-Cottrell locks and Hirth locks jointly governed the formation mechanism of machined surface. To demonstrate the feasibility and effectiveness of this proposed cutting strategy, the fabrication of periodic sinusoidal microstructures under constant forces was successfully realized on the microsphere surface. Furthermore, three-dimensional sin-shaped ripples required variable forces controlling were achieved with high-precision surface quality. The cross-sectional topography of obtained ripples corroborated the geometry of used multi-tip diamond (MTD) tool. In particular, the processing parameters, including the time period of loading forces and cutting speeds, determine the expected wavelength of ripples and play a central role in the surface machining accuracy.

Keywords:

Multi-tip diamond tool cutting, force modulation, three-dimensional sin-shaped ripples, MD simulation

1. INTRODUCTION

The engineered and controllable surface texturing has attracted much attention and found to be received as functional microstructures due to their significant value in both commercial and industrial applications. Anti-reflective property demonstrates that the periodic nanostructured surface help improve light transmission efficiency over various wavelengths and increase anti reflection ability over a wide range of incident angles[1]. Superhydrophobic feature results in water droplets easily rolling off from the lotus leaf surface due to hierarchal nanoscale humps attached with nanometer-scale hairs [2, 3]. Surface enhanced Raman scattering (SERS) requires the substrate surface roughness to excite surface plasmons for strengthening the electromagnetic effect through amplifying optical phonons[4-6]. The desired nanofeatures on the heated surface in pool boiling process are indispensable for getting a high heat transfer coefficient

between heat source and cooling liquid[7, 8]. Nanostructures, such as surface protrusions, provide more regions as active nucleation sites, while either increasing the critical heat flux or reducing the wall superheat[9, 10]. More importantly, hydrodynamic instabilities growth caused by surface defects of periodic sinusoidal ripples has been played a significant role in the failure of inertial confinement fusion (ICF) implosion performance[11, 12]. Many research projects are motivated to simulate the implosion weakening process by the artificial manufacturing of sin-shaped ripples on the microsphere surface[13].

There are several existing nanofabrication approaches to produce nanostructured surface, including lithography, nanocoining, bio-templates and etching. Currently, the interference lithography is the most general technique to create periodic arrays due to the exhibition of high quality and fidelity nanofeatures. However, the involvement of complicated production steps requires a quite long manufacturing duration, even consuming 11 hours in some lithographic process[14]. Although researchers assume that nanocoining proposes a rapid machining process for sub-micrometer surface using a diamond die, the issue of distortion and smearing brings much trouble to the formed nanofeatures precision because of the motion mismatch between the die and the workpiece surface[15]. Different from photonic and physical fabrication approach, bio-templates employs a biological mold with the expected nanostructures to generate subwavelength replications[16]. Etching techniques can be also regarded as an effective method to create moth-eye structures on the wafer surface by using silica crystal arrays masks[17]. Most of these methods need to prepare a high-quality mold and are not easy to generate nanostructured surface with various topographies, especially for processing on nonplanar surfaces. Thus, ultra-precision diamond turning using textured tools has been proven as a promising mechanical cutting approach for generating three-dimensional (3D) microstructures on curved or microsphere surface[18, 19]. Diversities of tool geometries, for example triangular, rectangular or other complicated shapes designed, offer an opportunity to fabricate functional microstructure surfaces with high productivity[20, 21]. In order to achieve high-accuracy microstructure surface with periodic sinusoidal ripples more efficiently, this paper proposes a novel strategy of

multi-tip diamond (MTD) tool cutting based on the force control principle.

The goal of this study is to realize the fabrication of 3D sin-shaped ripples with high-precision surface quality by using the multi-tip diamond tool, which is prepared by the focused ion beam (FIB) technique. The experiments are firstly carried out to obtain periodic sinusoidal ripples on the flat surface by keeping the normal forces constant, illustrating the influence of loading forces on the cutting depths and material removal states. As to further verify the capacities of cutting on the curved surface, the micro-balls are provided as samples for machining periodic sinusoidal ripples. Furthermore, the movement of dislocations nucleation is extremely difficult to uncover by experimental work. And MD simulation technique has been proven as an effective method to explore the atomic insight into the nanomachining on single crystal copper[22, 23]. Therefore, this paper utilizes MD simulation to explain the formation mechanism of machined surface during the process of MTD tool cutting on single crystal copper.

2. EXPERIMENTAL DETAILS

2.1 Experimental method

Figure 1 shows the schematic representation of machining periodic microstructures on the flat and curved surface by MTD tool under constant or variable forces. The experimental configuration and the cutting principle of proposed tip-based force control system are illustrated in the previous study[24]. This modified four-axis micromachining system consists of two high-precision stages (X,Y) driven by air floatation with the resolution of 1 nm, a motor driven coarse stage (Z) with the resolution of 0.5 μm and an air-bearing rotary stage (C) with radial rotation accuracy 0.26 μm. A PZT ceramics (PSt150/7/60VS12, COREMORROW, Harbin, China), a strain force sensor of 50-*g* capacity (LSB-200, FUTEK, Irvine, CA, USA) as well as a controller (UMAC, Delta Tau Data Systems, Los Angeles, CA, USA) were employed to be the parts of force modulation system, which maintained the normal forces exerted by the cutting tool on the workpiece surface constant. The schematic of proposed tip-based force control system describes a high-sensitivity force sensor integrated with the

PZT to realize accurately feedback control through the UMAC controller. As long as the difference existed between the measured contact force and the expected normal force is detected during the machining process, PZT actuator implement the displacement of extension or retraction to guarantee applied normal force between the cutting tool and the sample exactly the same as expected as well as constant.

In this study, a single-crystal copper piece of 5 mm × 5 mm with the surface orientation of [110] (Hefei Kejing Materials Technology Co., Ltd., China) is firstly selected as the sample. After machining on the flat surface, the experiments were extended to conduct on the surface of a copper coated micro-ball with the diameter of 1 mm, as shown in Figure 2, using the micro machine tool of Figure 1(A) from our previous research[25]. For the purpose of comparison of fabricated periodic nanostructures, such as topography and material removal state, a hollow thin-walled polymer micro-ball without coating copper is also used, which is illustrated in Figure 2 of previous study[25]. A commercial AFM (Dimension Icon; Bruker Corporation, USA) was used to observe the topography of machined periodic nanostructures by tapping mode. For scanning plane and curved surface, silicon tips (TESPA, Bruker Company, USA) with normal spring constant and resonance frequency were employed as 40 N/m and 320HZ and 0.2 N/m and 13 kHz, respectively.

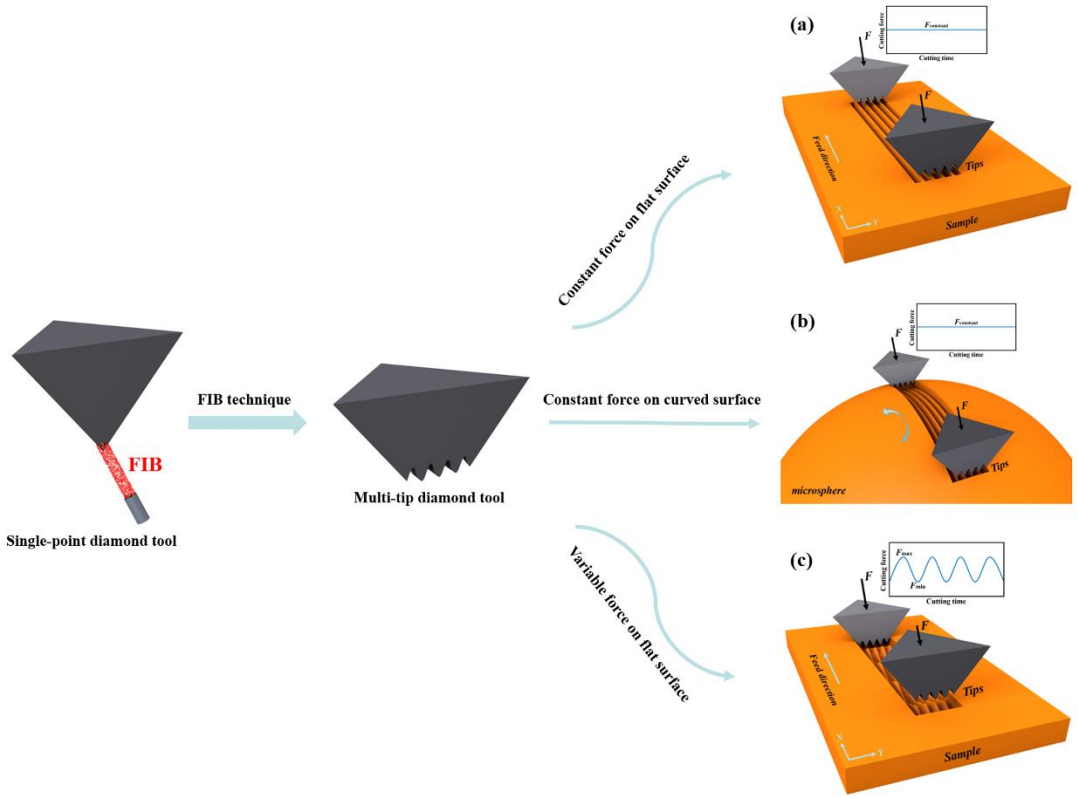

Fig. 1. Schematic representation of MTD tool cutting.

2.2 Preparation of the MTD tool

In this work, the MTD tool with periodic sinusoidal microstructures was produced by a dual-beam FIB system (FEI HeliosNanolab 600i). The form accuracy of MTD tool has considerable influence on its cutting performance, such as the topography of machined nanostructures and material removal state. In order to improve its form accuracy, it is essential to increase the charge conducting efficiency for suppressing the image drift. During the fabrication process, an acceleration voltage was fixed at 30 kV and an ion beam with a current of 24 pA scanned over the diamond tip to remove the redundant material. Meanwhile, the parameters of beam dwell time and overlap were set as 1 μs and 50%, respectively. As shown in Figure 2, a single-point diamond tool with a rake angle of 0°, a clearance angle of 6° and a tool included angle of 80° was prepared for fabricating the MTD tool. The period and amplitude of obtained MTD tool with sinusoidal microstructures can be considered as approximate 1 μm and 150 nm, respectively, which are illustrated in the scanning electron microscopy (SEM) image with a magnification 30000×. However, note that the amplitudes of tips of both sides

are smaller than those of the three tips in the middle. This phenomenon was attributed to the fact that during the manufacturing process of tips of both sides, less material redeposition and interference made material removal more efficient, and then certainly resulted in the tip edges of both sides smaller.

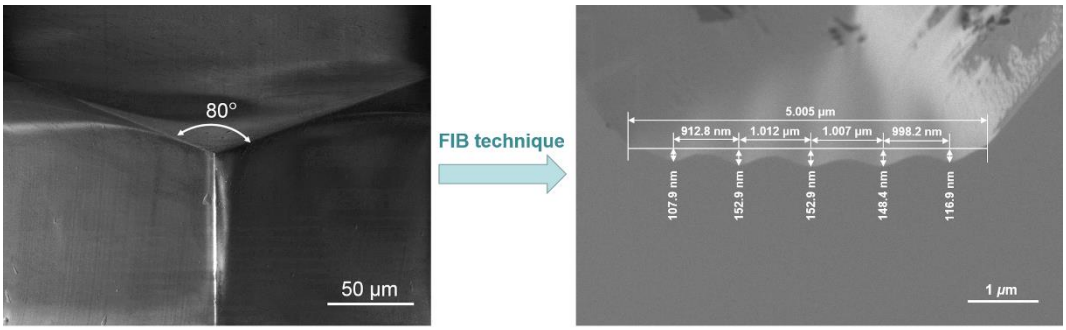

Fig. 2. SEM image of the MTD tool with periodic sinusoidal microstructures fabricated by FIB technique.

3. MD simulation methodology

In this study, MD simulation model of MTD tool cutting on single crystal copper was established, as shown in Figure 3. The MTD tool was build up with periodic sinusoidal microstructures. The dimension of single crystal copper substrate and MTD tool was 35.8 nm × 20.1 nm × 83.9 nm (totally 5,280,000 atoms) and 71.3 nm × 12.1 nm × 3.0 nm (55,816 atoms), respectively. The single crystal copper substrate consisted of newton atoms, thermostat atoms and boundary atoms, as illustrated in Figure 3(a). The initial temperature of single crystal copper substrate was kept 300 K via Nose-Hoover method[26]. The MTD tool was considered as rigid body during the nanoscratching process and the cutting direction was along with negative X axle direction with cutting velocity of 50 m/s. Additionally, the classic Tersoff potential function was selected to describe the MTD tool[27] and the EAM potential function was employed to calculate the atomic interactions of single crystal copper substrate[28, 29]. The atomic interaction between MTD tool and single crystal copper substrate was described by Morse potential function[30]. MD simulations of MTD tool cutting of single crystal copper were carried out in an open source code large-scale atomic/molecular massively parallel simulator (LAMMPS)[31] under NVE ensemble.

Open Visualization Tool (OVITO) software[32] was utilized to visualize the results of MD simulations. The detailed simulation parameters are indicated in Table 1.

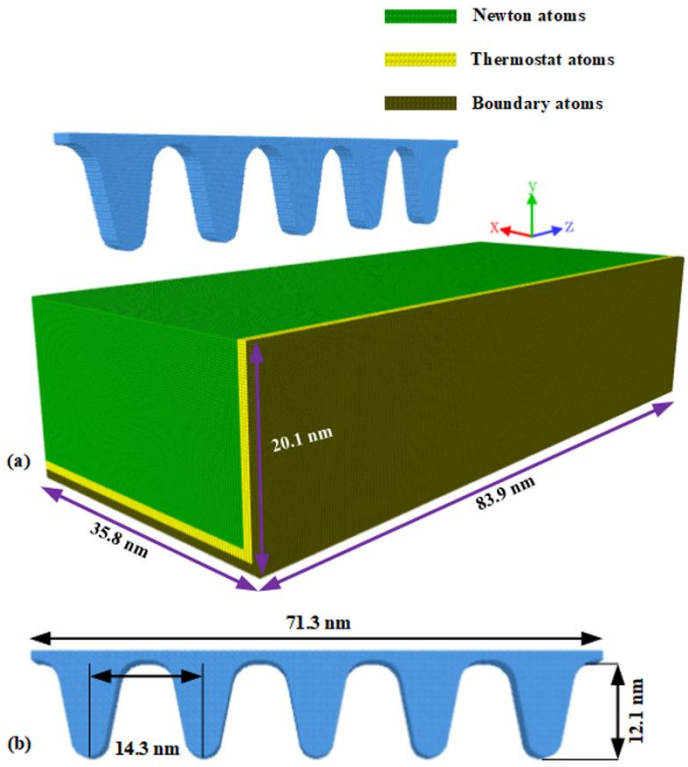

Fig. 3. (a) 3D model of MTD tool nanoscratching on single crystal copper, (b) MTD tool geometry.

Table 1. MD Simulation parameters.

Copper lattice structure	Face centered cubic (FCC)
Copper lattice constant	3.61 Å
Atom numbers of copper substrate	5,280,000
Substrate dimensions	35.8 nm × 20.1 nm × 83.9 nm
Machining tool	Cubic diamond
Diamond lattice constant	3.57 Å
Atom numbers of the machining tool	55,816
Machining tool dimensions	71.3 nm × 12.1 nm × 3.0 nm
Machining depth	2.1 nm
Machining distance	15 nm
Machining velocity	50 m/s

Machining lattice plane	(1 1 0)
Machining direction	[0 0 1]
Equilibration temperature	300 K
Potential functions	Hybrid (Tersoff, Morse, EAM)
Boundary condition	Periodic, shrink-wrapped and periodic along X, Y and Z directions
Timestep	1 fs

4. RESULTS AND DISCUSSION

4.1 Fabrication on flat surface under constant forces

On the basis of proposed force-feedback control strategy, the experiments of periodic sinusoidal microgrooves cutting were firstly conducted on a flat copper surface using the MTD tool under constant forces, as shown in Figure 1(a). In order to investigate the effect of normal cutting forces on machining mechanism, including material removal state and machining defects, the cutting forces were loaded over a wide range from 3mN to 17mN and kept constant during the whole scratching process. The cutting length and feed speed are set as 0.75 *mm* and 75 μm/*s*, respectively.

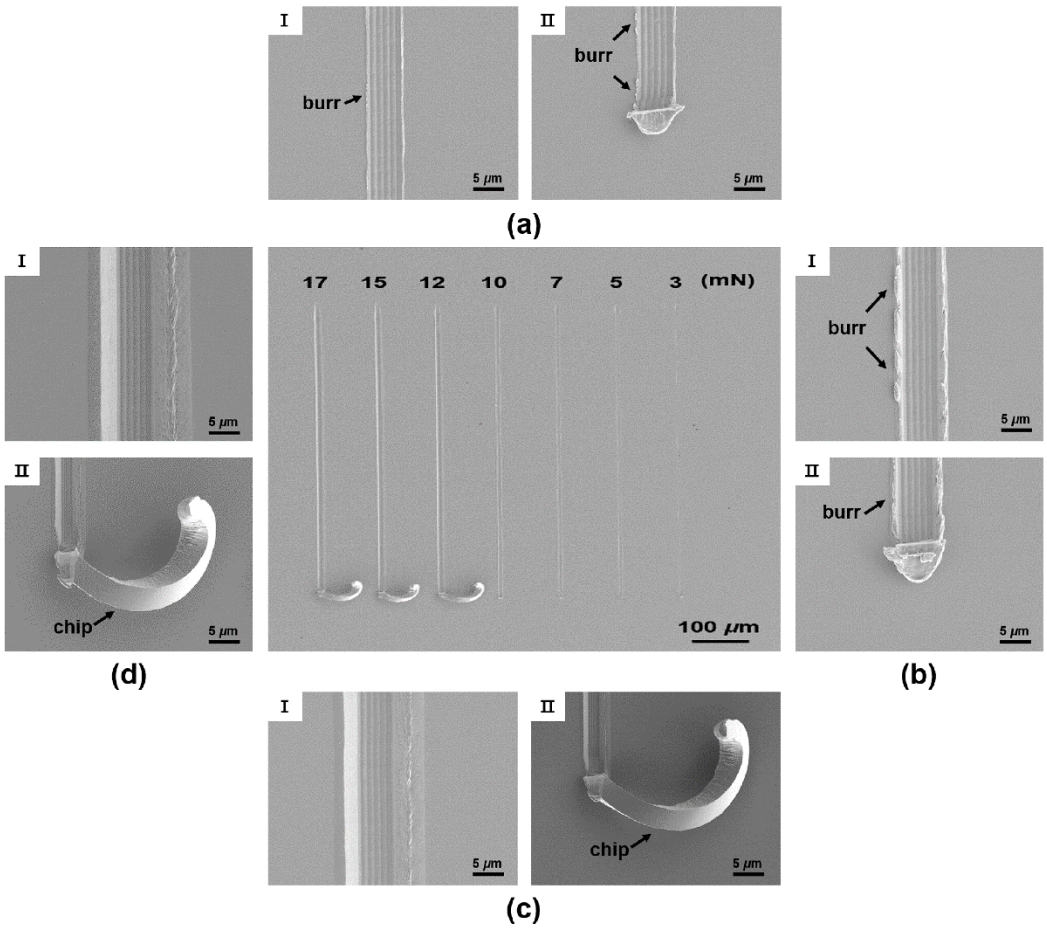

Fig. 4. Overall and local SEM images of sinusoidal microgrooves machined on the flat copper surface with respect to the cutting forces: (a) 5 mN, (b) 10 mN, (c) 12 mN and (d) 17 mN.

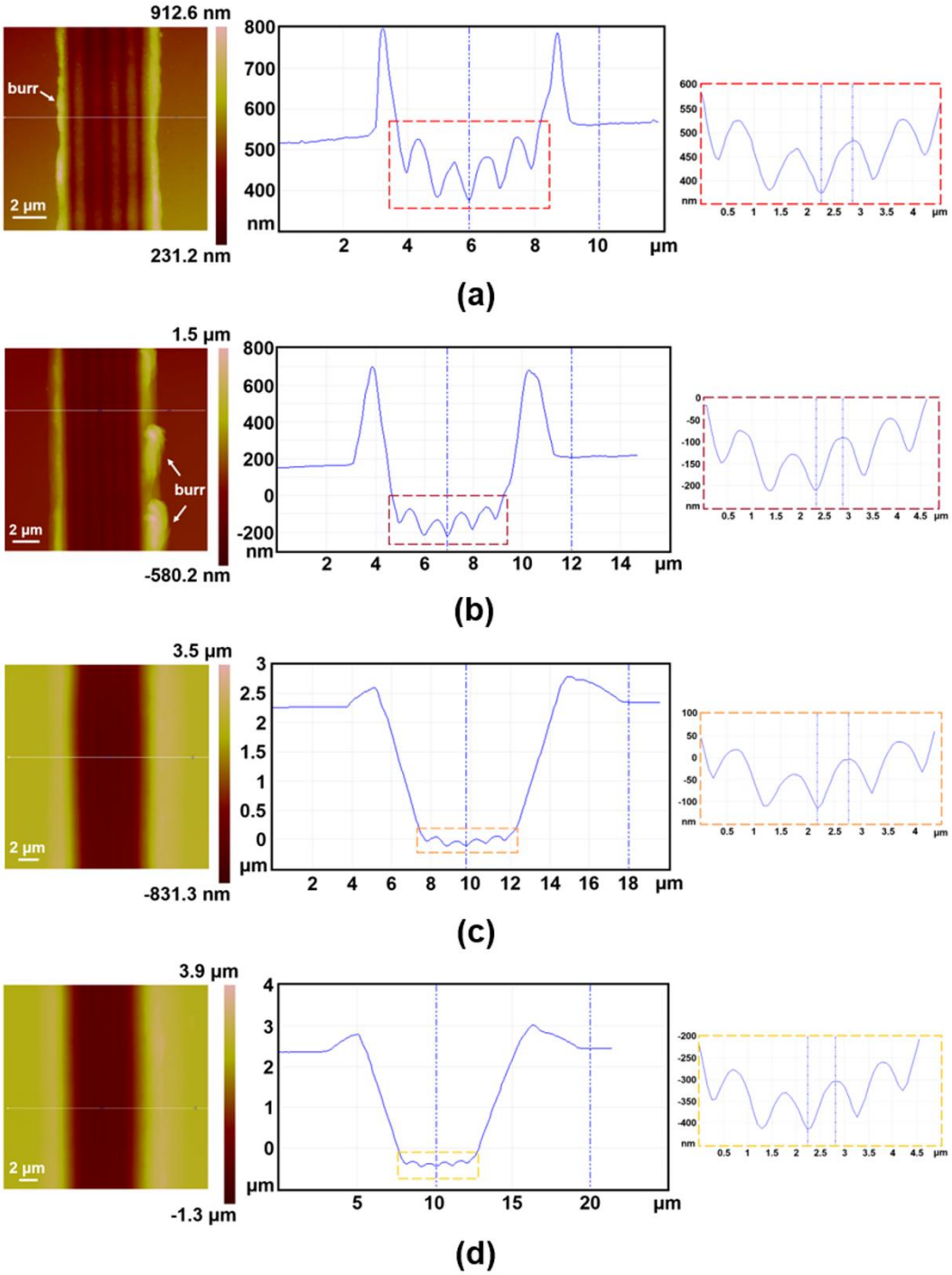

Fig. 5. AFM images of periodic sinusoidal microgrooves machined on the flat copper surface corresponding to the cutting forces: (a) 5 mN, (b) 10 mN, (c) 12 mN and (d) 17 mN.

The SEM and AFM images of machined microgrooves with respect to the setting normal forces of 5, 10, 12, 17 mN are shown in Figure 4 and Figure 5, respectively. And the images I and II in Figure 4 present the middle and end positions of each

microgroove, respectively. Two types of machining processes are distinguished according to the depths of cut. One case is that part of the tips is beneath the sample surface when the cutting depth is less than 150 nm of the tip height, the other is that the tips are completely surrounded by the sample as large depth cutting. In general, the obtained periodic sinusoidal microgrooves coincided with the geometry of used MTD tool quite well, as shown in the section profiles of AFM images. However, as evident from SEM images I and II in Figure 4(a) and (b) as well as AFM images in Figure 5(a) and (b), apparent side burrs distributed on the edge of machined microgrooves when the depths of cut were smaller than 468 nm. This might be attributed to the fact that as applying MTD tool cutting, the dislocation pile-ups took place beneath the tool tips due to the presence of overlap effect. Moreover, large pile-up was achieved by the accumulation of material bulge on both edges of machined microgrooves. With the increase of cutting forces to larger than 12mN, the images II in Figure 4(c) and (d) revealed that side burrs disappeared and the formation of C-shaped chips were observed clearly. This phenomenon can be explained as the larger the cutting depth, the larger range of deformed layer, and definitely significant dislocation pile-ups, which made the removed materials between the tips as well as in front of each tip flow up. Most importantly, along with the built-up volume of each cutting tip increasing, they eventually merged into one big chip. That is to say, when a depth of cut reaches a certain cutting thickness, side burrs no longer adhere to the edge of machined microgrooves, but accumulate to form chips. Thus, the above analysis indicated that there existed a critical value of depth of cut, which was closely responsible for the change of material removal state from plowing along with side burrs to generation of cutting chips.

In addition, the influence of applied cutting forces on depths of cut is plotted in Figure 6. When the material removal state was the same, i.e., plowing for loading forces smaller than 10 mN and cutting chips for loading forces larger than 12 mN, the cutting depths increased linearly with the increase of cutting forces. However, note that when the loading forces increased from 10 mN to 12 mN, the machined depth was evaluated to dramatically increase from 0.47 μm to 2.2 μm due to the appearance of cutting chips.

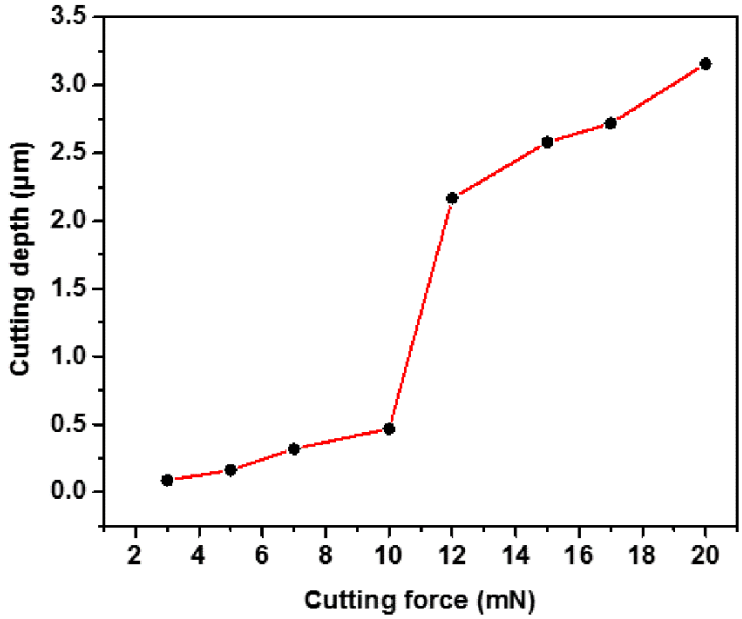

Fig. 6. Relationship between cutting forces and depths of cut on a flat copper surface.

4.2 Fabrication on curved surface under constant forces

As to further explore the possibility of machining periodic sinusoidal ripples on the curved surface by MTD tool under constant forces, as shown in Figure 1(b), the experiments were extended to the copper coated microsphere surface. Figure 7 shows that the diameter and thickness of such a hollow thin-walled microsphere are about 1 mm and 50 μm, respectively. Different from single-tip tool cutting, the most difficult problem is to align the MTD tool with the microsphere center for guaranteeing each tip in contact with microsphere surface during the cutting process. More importantly, it is essential to make the microsphere center coincide with the spindle rotation center, which is critical to the machining accuracy and implemented by the approach of optical capture software as described in the previous study[33]. Refer to Figure 6 of the force-depth relationship in plane scratching, the normal force was applied to 25 mN for getting larger cutting depth. The rotating speed of microsphere was set as 6 °/s, so that the processing efficiency can be improved as much as possible while considering the stability and machined surface quality. It was worthy of notice from Figure 7 that the periodic sinusoidal ripples were successfully achieved on different annuli of microsphere surface. The continuous ribbon chips were clearly observed and flowed out from the rake face of cutting tool. As provided in AFM image of Figure 7, the

wavelength and the peak-to-valley amplitude of machined ripples were measured to be approximate 1μm and 120nm, respectively, which exactly matched the shape of MTD tool. These positive results will be of great interest for the future application of manufacturing artificial surface defects on target ball surface used in ICF experiments and promoting the development of Rayleigh-Taylor instability research.

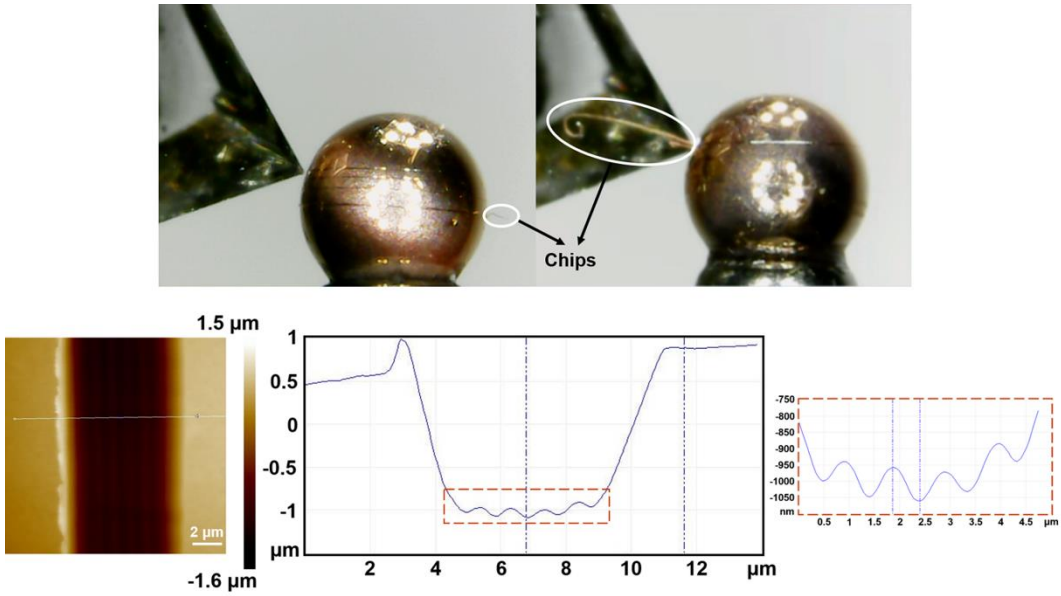

Fig. 7. Optical image of machining process on the copper coated micro-ball surface and AFM image of machined ripple.

4.3 Fabrication of three-dimensional sine-shaped ripples under variable forces.

Hydrodynamic instability growth in ICF capsules is anomalously susceptive to the distribution of sinusoidal ripples specified above a certain size. Typical specification is on the order of above 60 μm in wavelength and 0.8 to 2 μm in depth[11]. Demanding for the simulations of thermonuclear ignition motivated the fabrication of 3D sin-shaped ripples that meet the requirements of engineered surface defects. Thus, the experiments were carried out on the Cu (110) plane using MTD tool under variable forces, as presented in Figure 1(c). In order to achieve three-dimensional sin-shaped ripples through single scratching by using the MTD tool, the cutting forces between the tips and workpiece need to vary as a sinusoidal curve, where the peak and valley of reference forces were set as 12 mN and 10 mN, respectively. The time period of force

signals, that is, the loading and unloading rate, greatly influence the surface quality of machined sin-shaped ripples. The cutting speed is also critical to the surface roughness and keeps constant during the cutting process. Furthermore, the wavelength of ripples is determined by both the time period of sine force signals and cutting speeds, and the effect of these two key processing parameters on the machining accuracy of sinusoidal form of ripples is discussed in the following research.

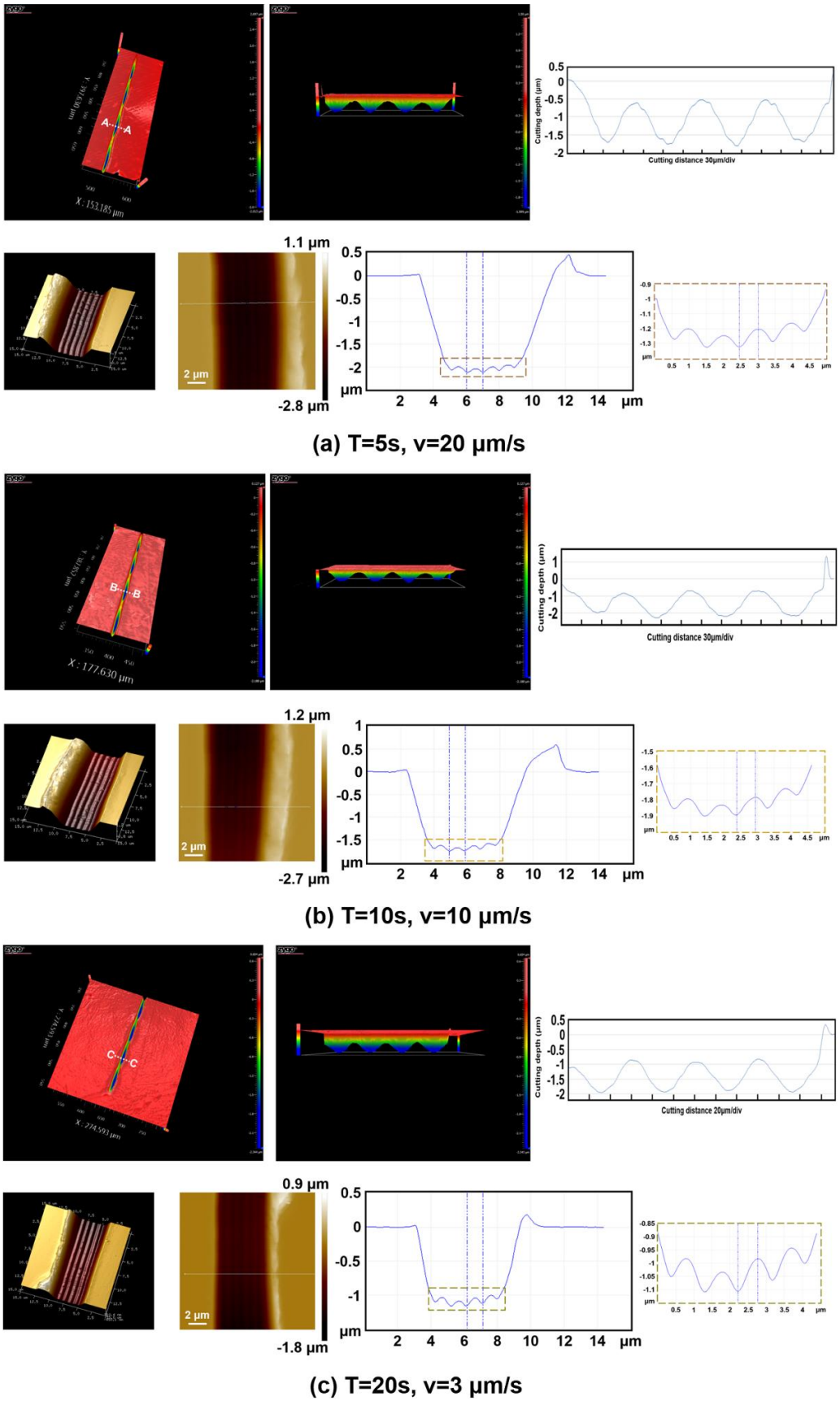

Fig. 8. Surface profile and AFM cross-sectional images of the ripples machined with different time periods of force signals and cutting speeds.

To set three groups of the time period of reference forces and cutting speeds, the 3D sin-shaped ripples with different features were successfully achieved, as shown in Figure 8. The longitudinal section topography of machined ripples is provided by a white light interferometer (ZYGO, NewView^{TM} 8200) due to the large measurement range of 830×830 μm. However, the laterally resolution of surface profiler is just 815 nm, which is close to the width of each microgroove. In view of this, the cross-sectional morphology is measured by AFM. It could be seen that five microgrooves obtained by single scratching with MTD tool formed periodic sinusoidal microstructures in cross direction. As shown in Figure 8(a), when the time period of force signal and the cutting speed were set as 5s and 20 μm/s, respectively, the wavelength of 102 μm was consistent with the theoretical value. The cutting depth formed a sinusoidal curve, where the peak and valley reached 1.91 μm and 0.56 μm, respectively. The machined surface quality was evaluated to exist some errors of the depth, which could be found in the longitudinal section topography and also from 3D image of cross section. This was primarily attributed to the fact that rapid loading and unloading from valley to peak of force signal as well as larger cutting speed had a significant influence on the machined surface quality. More specifically, during the machining process under variable forces, the ability of tracking reference force signals turns to be particularly critical. As to improve the machining accuracy, the time period of force signal increased to 10s and meanwhile, the cutting speed decreased to 10 μm/s. The amplitude of obtained sin-shaped ripple was approximately 1.32 μm and the wavelength was 101 μm. As evident from the side view of surface profile in Figure 8(b), the machined surface quality had been enhanced obviously. For further reducing the surface roughness of ripples, the time period of force signal and the cutting speed were set as 20s and 3 μm/s, respectively. The depth of cut was evaluated to be 1.22 μm, which estimated from a sine curve with a peak of 1.98 μm and a valley of 0.76 μm. And the wavelength of 60 μm exactly coincided with the theoretical computational value. The surface topography of ripples appeared to be much smoother and less uneven area on sin-shaped curve, which can be clearly observed from the longitudinal section curve and 3D cross-sectional AFM images in Figure 8(c). On the analysis of above results, the critical

values of time period of force signals had been verified to be from 5s to 20s, while the cutting speed should be controlled between 3 μm/s and 20 μm/s. It implied that the wavelength of ripples could be obtained from the shortest 15 μm to the longest 400 μm. Finally, depending on the expected wavelengths, the fabrication of three-dimensional sin-shaped ripples with high precision surface quality was realized by the selection of appropriate processing parameters.

4.4 Surface formation mechanism during MTD tool cutting

Cross-sectional of machined periodic nanogrooves in MD simulation is shown in Figure 9. It should be noted that copper atoms only piled up on both sides of nanogrooves while no material side flow was observed in the middle three nanogrooves. In comparison with a single point diamond tip cutting[34], the scratching process by using MTD tool can be guaranteed to free of the effect of material side flow due to the nature of special cutting tool geometry. To this end, it is more likely to obtain a better surface integrity without material side flow when the distance between adjacent tips of MTD tool is less than a critical value. And this critical value relates to depth of cut (DOC) as well as cutting velocities[35]. Undoubtedly, surface formation mechanism has close dependence on the movement of defects in the sub-surface of machined substrate. For this reason, the generated defects in the sub-surface were analyzed in the following for explaining no material side flow observed during the MTD tool nanocutting process.

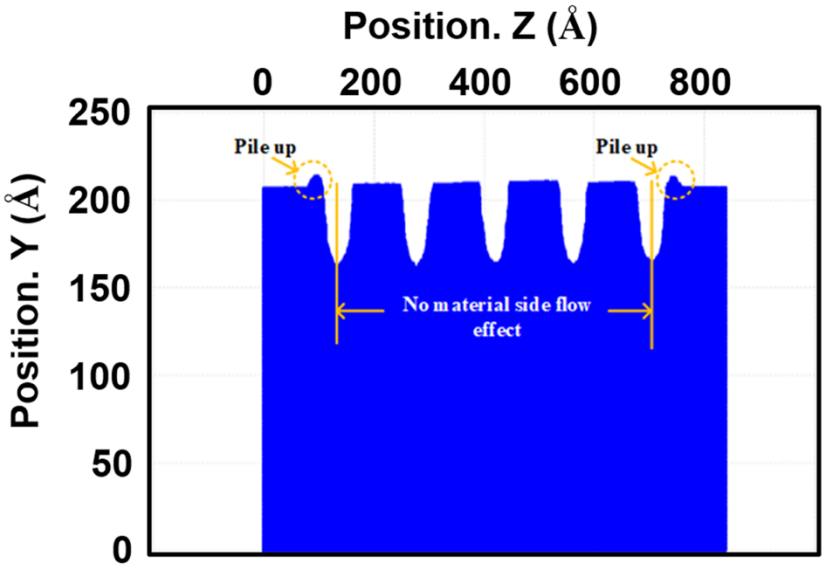

Fig. 9. Cross-sectional of machined periodic nanogrooves from MD simulation results.

Figure 10 shows the generation and propagation of dislocations and stacking faults (SFs) at scratching distance of 1 nm, 4 nm, 6 nm and 15 nm by employing the dislocation extraction algorithm (DXA) approach[36, 37]. It is evident to observe the five types of dislocations nucleation, e.g. 1/2<110> Perfect, 1/6<112> Shockley, 1/6<110> Stair-rod, 1/3<100> Hirth and 1/3<111> Frank during MTD tool nanoscratching on single crystal copper at cutting distance of 1 nm. Subsequently, a number of SFs are generated in the machined sub-surface of single crystal copper at scratching distance of 4 nm, 6 nm and 15 nm. Remarkably, a V-shaped defect is found in the sub-surface, as shown in Figure 11. The V-shaped defect is conducted by the annihilation of 1/6<112> Shockley dislocations to 1/6<110> Stair-rod dislocations, which can be represented as $1/6\,[\bar{1}2\bar{1}] + 1/6\,[2\bar{1}1] = 1/6\,[110]$. As a subsequent interaction, the Stair-rod dislocations with Burger vector $1/6\,[110]$ can react with Shockley dislocations with Burger vector $1/6\,[112]$ to create Frank dislocations with 1/3[111]. The formation of Stair-rod dislocations and Frank dislocations is named as Lomer-Cottrell (L-C)[38, 39]. Additionally, the dissociation reaction of Hirth dislocations can be represented as $1/3\,[100] = 1/6\,[1\bar{2}1] + 1/6\,[12\bar{1}]$, which is universally known as Hirth lock[40].

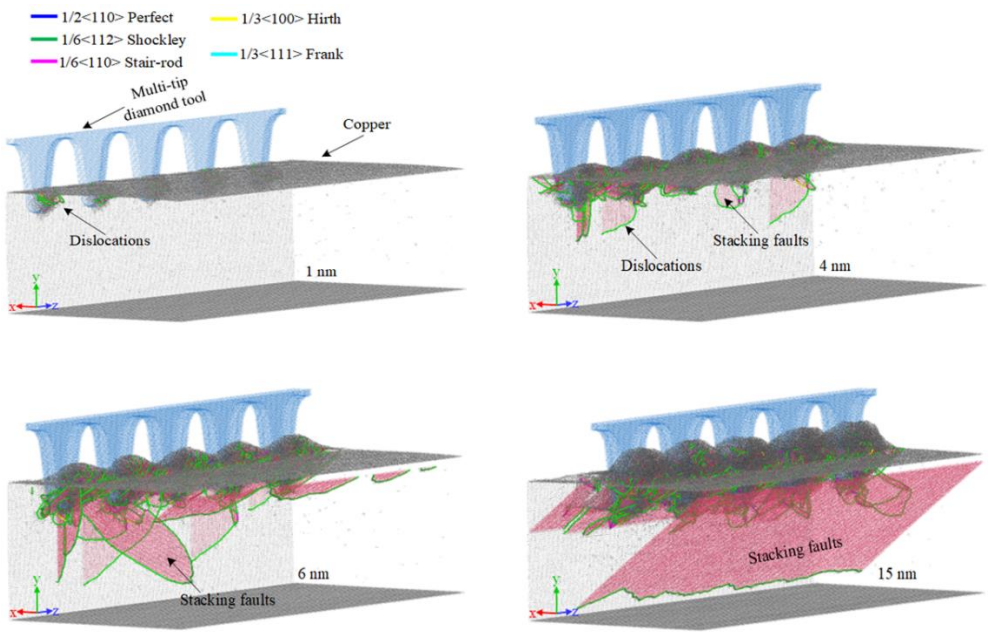

Fig. 10. Atomic snapshots of dislocations and stacking faults at scratching distance of 1 nm, 4 nm, 6 nm and 15 nm.

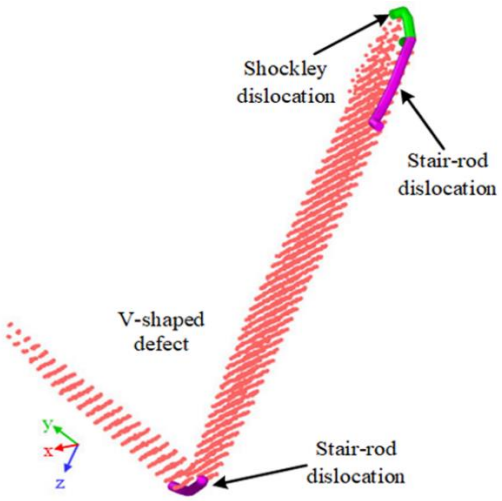

Fig. 11. Atomic snapshot of V-shaped defect.

Apart from the SFs and V-shaped defect, the dislocation junction, Stair-rod steps, dislocation loops and dislocation node are observed under the sub-surface, as shown in Figure 12. Formation of the dislocation junction and dislocation node can be attributed to the storage of the energy. With the proceeding of MTD tool nanoscratching, the energy within the junction and node is released to split into the dislocation segments. Moreover, formation of the dislocation loop and stair-rod steps would definitely hinder the movement of dislocations, resulting in the sharp increase of cutting resistance.

Meanwhile, the variation of dislocation density is presented in Figure 14. The density of 1/6<112> Shockley dislocation went up rapidly before the scratching distance of 6 nm and kept fluctuation between 6 nm and 15 nm. The reason of fluctuation may be ascribed to Shockley dislocation dissociation and annihilation to 1/2<110> Perfect, 1/6<110> Stair-rod, 1/3<100> Hirth and 1/3<111> Frank dislocation. Furthermore, Figure 13 suggests that the density of Shockley dislocation is the most, followed by Stair-rod dislocation, Hirth dislocation, Perfect dislocation and Frank dislocation. During multi-tip diamond tool-based nanomachining process, plenty of copper atoms have been displaced from one steady site to another. Consequently, a number of Shockley dislocations have been formed. Then, the pair of Shockley dislocation can result in the formation of SFs, which is the reason of why the Shockley dislocation is the dominated dislocation.

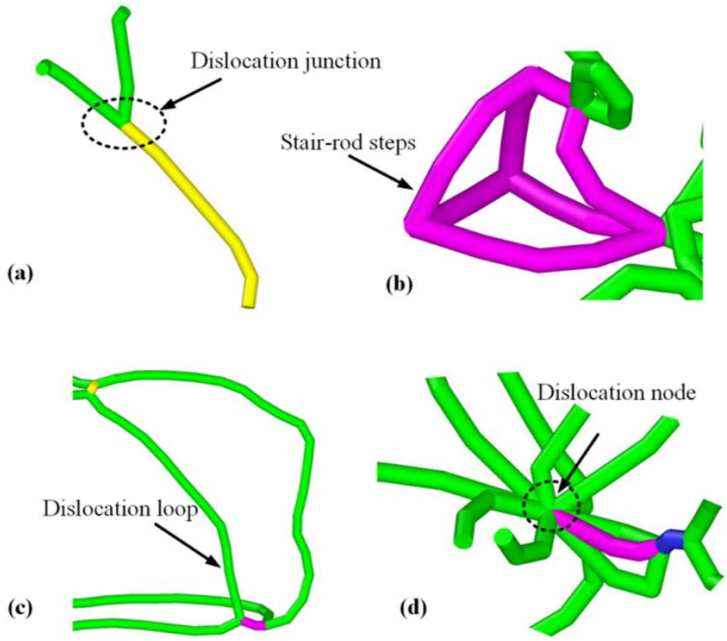

Fig. 12. Evolution of dislocations in the sub-surface of single crystal copper during MTD tool nanoscratching.

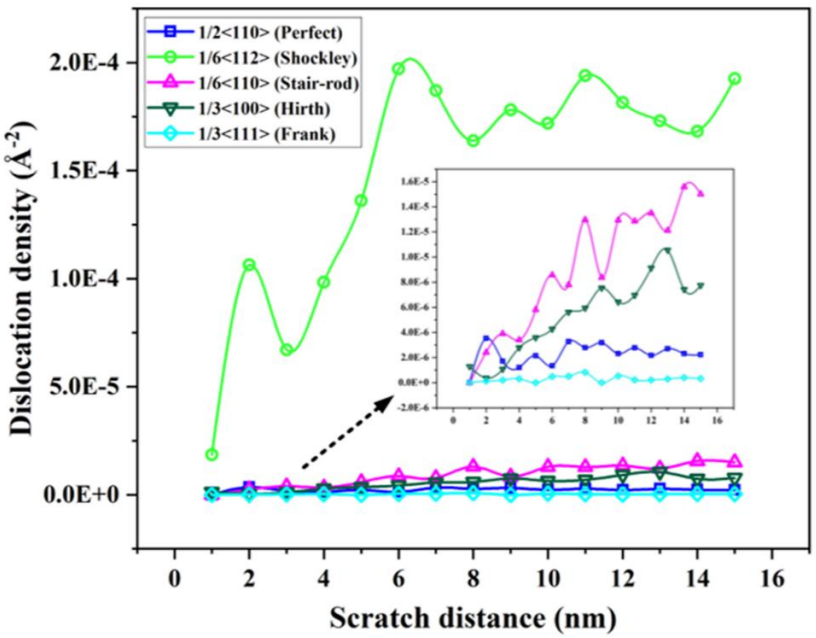

Fig. 13. Variation of density of five types of dislocations.

Stress is regarded as a significant role for inducing the dislocations nucleation and formation of SFs. Figure 14 shows the hydrostatic stress distribution of cutting zone of single crystal copper. It is clear to see that the substrate demonstrates obvious surface stress effect, that is, the substrate surface has large tensile stress up to 9.2 GPa. The area of large compressive stress is the primary shear slip zone, where the generous stacking faults generates. Much more interestingly, dual high stress spots I and II are found inside the substrate, which indicates the incipient formation place of perfect SFs (see Figure 10 at scratching distance of 15 nm). Additionally, figure 14 demonstrates the high stress spots are close to the boundary layer of the substrate. Therefore, the formation of high-stress spots may also be due to the influence of boundary layer apart from the multi-tip diamond tool extrusion effect.

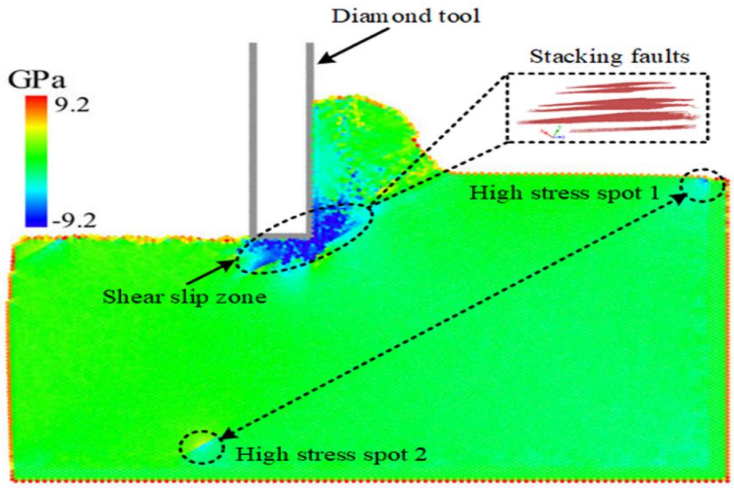

Fig. 14. Hydrostatic stress distribution of cutting zone of single crystal copper.

5. CONCLUSIONS

The most contribution of this study is to propose a novel approach of fabricating three-dimensional sin-shaped ripples using the multi-tip diamond tool under the variable forces. The experimental work was firstly carried out to investigate the influence of MTD tool cutting on single crystal copper surface under constant forces. The effect of applied normal forces on the depth of cut was explored, and the cutting depths determined the material removal states. Furthermore, MD simulations have been utilized to give the atoms inside into the formation mechanism of machined surface when using the MTD tool cutting. The conclusions are drawn as follows:

(1) Periodic sinusoidal microstructures required in the ICF experiments were successfully achieved on the copper coated microsphere surface under constant forces. The cross-sectional topography of machined microstructures matches the geometry of used MTD tool quite well.

(2) The fabrication of 3D sin-shaped ripples on the flat copper surface demands the realization of variable forces control. The wavelengths of ripples measured experimentally are in full agreement with the theoretical values obtained from the calculation of time period of sine force signals and cutting speeds.

(3) Under the action of variable forces, the influence of processing parameters, such as the time period of loading forces and cutting speeds, on the surface quality of machined 3D sin-shaped ripples are revealed. The desired wavelengths in an

optimal range (from the shortest 15 μm to the longest 400 μm) can be obtained by selecting the appropriate processing parameters, while guaranteeing the high accuracy of surface quality.

(4) The phenomenon of no material side flow was observed during MD simulations, owing to the fact that formation of machined surface was governed by the movement of generated defects in the sub-surface, such as SFs, Lomer-Cottrell locks and Hirth locks. This result is consistent with experimental work and indicates that MTD tool cutting based on the force modulation approach may be considered as a remarkable candidate for scale-up machining of periodic nanostructures.

Acknowledgement

This work was supported by the National Natural Science Foundation of China (52035004, 51911530206), Natural Science Foundation of Heilongjiang Province of China (YQ2020E015), Self-Planned Task (NO. SKLRS202001C) of State Key Laboratory of Robotics and System (HIT), "Youth Talent Support Project" of the Chinese Association for Science and Technology and the Fundamental Research Funds for the Central Universities.

XL would like to thank EPSRC (EP/K018345/1, EP/T024844/1) and the Royal Society-NSFC international exchange programme (IEC\NSFC\181474) to provide financial support to this research. SG is particularly thankful to the research support provided by the UKRI via Grants No. EP/L016567/1, EP/S013652/1, EP/T001100/1, EP/S036180/1, EP/T024607/1, TFIN+ Feasibility study award to LSBU (EP/V026402/1), the Royal Academy of Engineering via Grants No. IAPP18-19\295 and TSP1332, EURAMET EMPIR A185 (2018), the EU Cost Action (CA15102, CA18125, CA18224 and CA16235) and the Newton Fellowship award from the Royal Society (NIF\R1\191571). This work also accessed the Isambard Bristol, UK supercomputing service via Resource Allocation Panel (RAP) as well as ARCHER resources (Project e648). The authors also acknowledge the use of the EPSRC (EP/K000586/1) funded ARCHIE-WeSt High-Performance Computer at the University of Strathclyde.

References

[1] E.M. Zdanowicz, Nanocoining Sub-Micron Features, Dissertations & Theses - Gradworks, (2013).

[2] L. Zhang, Z. Zhou, B. Cheng, J.M. Desimone, E.T. Samulski, Superhydrophobic behavior of a perfluoropolyether lotus-leaf-like topography, Langmuir the Acs Journal of Surfaces & Colloids, 22 (2006) 8576.

[3] M.H. Sun, C.X. Luo, L.P. Xu, H. Ji, O.Y. Qi, D.P. Yu, Y. Chen, Artificial lotus leaf by nanocasting, Langmuir, 21 (2005) 8978-8981.

[4] M. Sun, C. Qian, W. Wu, W. Yu, Y. Wang, H. Mao, Self-assembly nanoparticle based tripetaloid structure arrays as surface-enhanced Raman scattering substrates, Nanotechnology, 23 (2012).

[5] P. Bruno, Surface-enhanced Raman scattering - Physics and applications, Topics in applied physics, 103 (2006) 40.

[6] J. Zhang, Y. Yan, P. Miao, J. Cai, Fabrication of gold-coated PDMS surfaces with arrayed triangular micro/nanopyramids for use as SERS substrates, Beilstein Journal of Nanotechnology, 8 (2017) 2271-2282.

[7] T.J. Hendricks, S. Krishnan, C.H. Choi, C.H. Chang, B. Paul, Enhancement of pool-boiling heat transfer using nanostructured surfaces on aluminum and copper, Int. J. Heat Mass Transf., 53 (2010) 3357-3365.

[8] B. Stutz, C.H.S. Morceli, M.D. da Silva, S. Cioulachtjian, J. Bonjour, Influence of nanoparticle surface coating on pool boiling, Exp. Therm. Fluid Sci., 35 (2011) 1239-1249.

[9] S. Vemuri, K.J. Kim, Pool boiling of saturated FC-72 on nano-porous surface, Int. Commun. Heat Mass Transf., 32 (2005) 27-31.

[10] S.H. Li, R. Furberg, M.S. Toprak, B. Palm, M. Muhammed, Nature-inspired boiling enhancement by novel nanostructured macroporous surfaces, Adv. Funct. Mater., 18 (2008) 2215-2220.

[11] L.C. Carlson, E.L. Alfonso, H. Huang, A. Nikroo, M.E. Schoff, M.N. Emerich, T. Bunn, N.A. Antipa, J.B. Horner, AUTOMATION OF NIF TARGET CHARACTERIZATION AND LASER ABLATION OF DOMES USING THE 4PI SYSTEM, Fusion Science and Technology, 67 (2015) 762-770.

[12] V.A. Smalyuk, M. Barrios, J.A. Caggiano, D.T. Casey, C.J. Cerjan, D.S. Clark, Hydrodynamic instability growth and mix experiments at the National Ignition Facility, Phys. Plasmas, 21 (2014) 8.

[13] K.S. Raman, V.A. Smalyuk, D.T. Casey, S.W. Haan, D.E. Hoover, O.A. Hurricane, J.J. Kroll, A. Nikroo, J.L. Peterson, B.A. Remington, H.F. Robey, D.S. Clark, B.A. Hammel, O.L. Landen, M.M. Marinak, D.H. Munro, K.J. Peterson, J. Salmonson, An in-flight radiography platform to measure hydrodynamic instability growth in inertial confinement fusion capsules at the National Ignition Facility, Phys. Plasmas, 21 (2014) 21.

[14] K.C. Park, H.J. Choi, C.H. Chang, R.E. Cohen, G.H. McKinley, G. Barbastathis, Nanotextured Silica Surfaces with Robust Superhydrophobicity and Omnidirectional Broadband Supertransmissivity, ACS Nano, 6 (2012) 3789-3799.

[15] W. Nowak, Ultrasonic Nanocoining of Sub-micrometer Surface Features,

Dissertations & Theses - Gradworks, (2014).

[16] G.Y. Xie, G.M. Zhang, F. Lin, J. Zhang, Z.F. Liu, S.C. Mu, The fabrication of subwavelength anti-reflective nanostructures using a bio-template, Nanotechnology, 19 (2008).

[17] C.H. Sun, P. Jiang, B. Jiang, Broadband moth-eye antireflection coatings on silicon, Applied Physics Letters, 92 (2008).

[18] M.A. Davies, C.J. Evans, S.R. Patterson, R. Vohra, B.C. Bergner, Application of precision diamond machining to the manufacture of micro-photonics components, in: E.B. Kley, H.P. Herzig (Eds.) Lithographic and Micromachining Techniques for Optical Component Fabrication Ii, Spie-Int Soc Optical Engineering, Bellingham, 2003, pp. 94-108.

[19] Y. Picard, D.P. Adams, M.J. Vasile, M.B. Ritchey, Focused ion beam-shaped microtools for ultra-precision machining of cylindrical components, Precis. Eng.-J. Int. Soc. Precis. Eng. Nanotechnol., 27 (2003) 59-69.

[20] X. Ding, G.C. Lim, C.K. Cheng, D.L. Butler, K.C. Shaw, K. Liu, W.S. Fong, Fabrication of a micro-size diamond tool using a focused ion beam, J. Micromech. Microeng., 18 (2008) 10.

[21] Z.W. Xu, F.Z. Fang, S.J. Zhang, X.D. Zhang, X.T. Hu, Y.Q. Fu, L. Li, Fabrication of micro DOE using micro tools shaped with focused ion beam, Opt. Express, 18 (2010) 8025-8032.

[22] S. Goel, M. Knaggs, G. Goel, X.W. Zhou, H.M. Upadhyaya, V.K. Thakur, V. Kumar, G. Bizarri, A. Tiwari, A. Murphy, A. Stukowski, A. Matthews, Horizons of

modern molecular dynamics simulation in digitalized solid freeform fabrication with advanced materials, Mater. Today Chem., 18 (2020) 15.

[23] S. Goel, X.C. Luo, A. Agrawal, R.L. Reuben, Diamond machining of silicon: A review of advances in molecular dynamics simulation, Int. J. Mach. Tools Manuf., 88 (2015) 131-164.

[24] Y. Yan, Y. Wang, J. Wang, Y. Geng, Effect of material removal state on the selection of theoretical models when scratching single-crystal copper using the load modulation approach, Proceedings of the Institution of Mechanical Engineers, Part B: Journal of Engineering Manufacture, 234 (2019) 720-729.

[25] Y.Z. Wang, Y.Q. Geng, Y.D. Yan, J.Q. Wang, Z. Fang, Robust model predictive control of a micro machine tool for tracking a periodic force signal, Optim. Control Appl. Methods, 41 (2020) 2037-2047.

[26] S. Nose., A Unified formulation of the constant-temperature molecular-dynamics methods, The Journal of Chemical Physics, 81 (1984) 511-519.

[27] Tersoff, J., Modeling solid-state chemistry: Interatomic potentials for multicomponent systems, Phys Rev B Condens Matter, 39 (1989) 5566-5568.

[28] M.S. Daw, M.I. Baskes, Semiempirical, Quantum Mechanical Calculation of Hydrogen Embrittlement in Metals, Physical Review Letters, 50 (1983) 1285-1288.

[29] M.S. Daw, M.I. Baskes, Embedded-atom method: Derivation and application to impurities, surfaces, and other defects in metals, Physical Review B Condensed Matter, 29 (1984) 6443-6453.

[30] Satoh, Akira, Stability of Various Molecular Dynamics Algorithms, Journal of

Fluids Engineering, 119 (1997) 476.

[31] S. Plimpton, Fast parallel algorithms for short-range molecular dynamics, (1993).

[32] A. Stukowski, Visualization and analysis of atomistic simulation data with OVITO-the Open Visualization Tool, Model. Simul. Mater. Sci. Eng., 18 (2010) 7.

[33] Y. Wang, Y. Geng, L. Guo, J. Wang, Z. Fang, Y. Yan, Study of machining indentations over the entire surface of a target ball using the force modulation approach, International Journal of Extreme Manufacturing, 3 (2021) 035102.

[34] Z. Tong, Y.C. Liang, X.Q. Jiang, X.C. Luo, An atomistic investigation on the mechanism of machining nanostructures when using single tip and multi-tip diamond tools, Appl. Surf. Sci., 290 (2014) 458-465.

[35] P.Z. Zhu, Y.Z. Hu, T.B. Ma, H. Wang, Study of AFM-based nanometric cutting process using molecular dynamics, Appl. Surf. Sci., 256 (2010) 7160-7165.

[36] A. Stukowski, K. Albe, Extracting dislocations and non-dislocation crystal defects from atomistic simulation data, Model. Simul. Mater. Sci. Eng., 18 (2010) 13.

[37] A. Stukowski, V.V. Bulatov, A. Arsenlis, Automated identification and indexing of dislocations in crystal interfaces, Model. Simul. Mater. Sci. Eng., 20 (2012) 16.

[38] T. Paulauskas, C. Buurma, E. Colegrove, B. Stafford, Z. Guo, M.K.Y. Chan, C. Sun, M.J. Kim, S. Sivananthan, R.F. Klie, Atomic scale study of polar Lomer-Cottrell and Hirth lock dislocation cores in CdTe, Acta Crystallogr. Sect. A, 70 (2014) 524-531.

[39] D.K. Mishra, M. Meraj, S.K. BadJena, S. Pal, Dislocation Interaction and V-Shaped Growth of the Distorted Structure During Nanoindentation of Cu20Ni20Al20Co20Fe20 (high-entropy alloy)-Coated Copper: A Molecular Dynamics Simulation-Based Study, Trans. Indian Inst. Met., 72 (2019) 167-180.

[40] L. Dupuy, M.C. Fivel, A study of dislocation junctions in FCC metals by an orientation dependent line tension model, Acta Mater., 50 (2002) 4873-4885.